Growth and immunity receptors compete for co-receptors to regulate balance in plants

Qiaorui Zhang, Canxi Chen, Jiayu Zou

Abstract

Plant growth and immunity share a common co-receptor. The receptor kinase BAK1 is recruited both into the BRI1–brassinosteroid growth complex and into the FLS2–flg22 immune complex, so the two pathways compete for a single, limited pool. How this competition is resolved sets the growth–immunity balance, but the quantitative mechanism has been missing.

We model the competition with an explicit two-step, mass-action ODE in which ligand–receptor binding is reversible and the ternary complex then recruits shared BAK1. Reversibility does not weaken binding; it caps the effective affinity at high ligand, so signalling is strong yet bounded. On this dynamics we build two-level decision heatmaps—over ligand concentrations and over receptor expression—and recover three antagonistic phenomena (BRI1-overexpression suppression, BAK1 rescue, and high-BR suppression) from pure competition alone, with no priming term. Parameter sampling assigns each biological knob its role: receptor stoichiometry gates whether antagonism occurs, downstream defence efficiency sets the switch point and the total-signal ceiling, and co-receptor affinity sets the saturation position.

The model reconciles the competing views that BAK1 is, or is not, growth-limiting as two readings of one decision surface, and it predicts a negative cross-reaction order measurable along a flg22 gradient. The growth–immunity switch is a tunable surface set by the scarcity and partitioning of a shared co-receptor.

Keywords: shared co-receptor BAK1; mass-action ODE; ligand–receptor reversibility and saturation; receptor stoichiometry; two-level decision heatmaps; growth–defense trade-off.

1 Introduction

Plants are sessile and cannot evade biotic stress, so every cell must continuously balance investment in growth against investment in immunity. These two programs act as a seesaw: resources and shared signalling components committed to one reduce the output of the other, a constraint known as the growth–defense trade-off [1, 2]. The trade-off is acute for agriculture, because breeding crops for strong disease resistance frequently penalises yield. The central question is how a plant cell computes this balance at the molecular level.

We address it in Arabidopsis thaliana, the canonical plant model, whose signalling gene families are conserved with those of major crops [3]. The receptors that govern both sides of the seesaw belong to the leucine-rich-repeat receptor-like kinase (LRR-RLK) family, the largest class of cell-surface receptors in plants [4, 5]. Growth is driven by BRI1, which perceives the steroid brassinosteroid, and basal immunity by FLS2, which perceives the bacterial flagellin epitope flg22.

Both receptors signal through the same SERK-family co-receptor, BAK1 (SERK3): BAK1 is recruited into the BRI1–brassinosteroid growth complex and into the FLS2–flg22 immune complex, making it the shared hub at which growth and defense pull against one another [6, 7]. Because BAK1 is shared and of limited abundance, the two pathways compete for it, and how this competition is resolved sets the growth–immunity balance.

Studying this competition experimentally is difficult. BAK1 and its partners are membrane proteins, which are hard to express, purify, and reconstitute in their native state, so receptor interactions are often resolved in vivo by imaging rather than by biochemistry [8]. The interaction data the field relies on come largely from in vitro extracellular-domain assays, or from curated databases that mix validated with predicted links and so carry false positives [9]. And although mathematical models have been built for single pathways—the brassinosteroid growth pathway [10], and the dynamics of brassinosteroid signalling more generally [11]—no model has yet captured how a shared, scarce co-receptor arbitrates between growth and immunity. The quantitative mechanism behind the trade-off is therefore still missing.

Here we build an explicit two-step, mass-action ODE model of BRI1 and FLS2 competing for shared BAK1, following the promiscuous-binding framework of Su et al. [12]. We show that the growth–immunity switch is set by the scarcity and partitioning of the co-receptor; we recover the three antagonistic phenomena of Belkhadir et al. [13] from competition alone; we reconcile the view that BAK1 is not growth-limiting, due to Albrecht et al. [14], with the competition view on a single decision surface; and we constrain the receptor geometry with the FLS2–flg22–BAK1 structure [15].

2 Model and methods

2.1 Explicit two-step reversible mass-action ODE

Each pathway forms a ternary complex through two reversible binding steps ($i = 1$ growth BL/BRI1, $i = 2$ defense flg22/FLS2; R_A = shared BAK1):

$$\text{step 1 } L_i + R_i \rightleftharpoons C_i \quad (k_{\text{on},i},\ k_{\text{off},i};\ K_{di} = k_{\text{off},i}/k_{\text{on},i})$$

$$\text{step 2 } C_i + R_A \rightleftharpoons T_i \quad (k^+_{A,i},\ k^-_{A,i};\ K_{iA} = k^+_{A,i}/k^-_{A,i})$$

Ligand L_i is treated as a constant bath (a scanned parameter), so each pathway tracks only the binary complex C_i and the ternary complex T_i; free receptor and free co-receptor follow from conservation:

$$R_i^{\text{free}} = R_{i,\text{tot}} - C_i - T_i, \qquad F = R_{A,\text{tot}} - T_1 - T_2$$

Mass action gives **4 ODEs** (the core change from earlier — writing the time derivatives and integrating):

$$\boxed{\begin{aligned} \dot{C}_i &= k_{\text{on},i} L_i R_i^{\text{free}} - k_{\text{off},i} C_i - k^+_{A,i} C_i F + k^-_{A,i} T_i \\ \dot{T}_i &= k^+_{A,i} C_i F - k^-_{A,i} T_i \end{aligned}}, \qquad S_1 = a_1 T_1,\ \ S_2 = a_2 T_2$$

Here a_i is the downstream signalling efficiency of a ternary complex. The system is dissipative and contractive (Jacobian eigenvalues have negative real part), so from any non-negative initial condition it monotonically approaches a **unique steady state** (Appendix A). Setting $\dot{C}_i = \dot{T}_i = 0$ and simplifying analytically yields the the earlier algebraic fixed point:

$$T_i = \frac{\alpha_i R_{i,\text{tot}} F}{1 + \alpha_i F}, \qquad \alpha_i = \frac{K_{iA} L_i}{K_{di} + L_i}$$

α_i is the **effective affinity** that folds the two steps: at low ligand ($L_i \ll K_{di}$), $\alpha_i \approx (K_{iA}/K_{di})L_i$ (the one-step linear form, the old Su form); at high ligand, $\alpha_i \to K_{iA}$ (the ligand–receptor step saturates). The key distinction this work: **we obtain this steady state by directly integrating the ODE, not by solving the algebraic equation**; the algebraic form is used only for verification (§3.1).

2.2 Numerical integration to steady state

Given parameters and initial conditions (all free: $C_i(0) = T_i(0) = 0$), integrate the ODE until $\max|\dot{C}_i, \dot{T}_i| < \text{tol}$. Two implementations cross-check each other:

- **Explicit Euler pseudo-time integration** (main computation): per-cell adaptive step $\Delta t = 1.2/\rho_i$ (ρ_i = upper bound on that cell's spectral radius). The dissipative system converges monotonically under Euler for $\Delta t < 2/\rho_i$, and the Euler fixed point = ODE fixed point = physical steady state; **each cell uses its own step**, so a

ligand grid with a large dynamic range is not dragged down by stiffness (a whole 61×61 grid integrates in < 1 s). All heatmaps and sampling use this.

- **`scipy.solve_ivp` (RK45)**: used for the time-course plot (§3.1 Fig. 1a), showing the true trajectory approaching steady state.

Rate values: $k_{\mathrm{on},i} = k_{A,i}^{+} = 1$ (setting only the time scale), $k_{\mathrm{off},i} = K_{di}$, $k_{A,i}^{-} = 1/K_{iA}$. **The steady state depends only on the ratios K_{di}, K_{iA}, not on the absolute rates** — so the rates can be chosen freely for good numerical behavior.

2.3 Reversibility and saturation

Does "ligand–receptor reversibility" change the model? Yes, in the denominator of α_i. The one-step linear $\alpha^{\mathrm{lin}} = (K_{iA}/K_{di})L$ grows without bound with L; the two-step reversible $\alpha = K_{iA}L/(K_{di} + L)$ **caps** at K_{iA} for $L \gg K_{di}$. The downstream consequence (Fig. 2): the one-step S_1 tends to $a_1 R_{1,\mathrm{tot}} = 2$ at high BL (receptor saturated by ligand), whereas the two-step model caps earlier at ≈ 0.72 (ligand can fall off the receptor, so the receptor is not saturated). In a sentence: **reversible ≠ weak, but "strong yet bounded"**. This is the origin of the reaction-order decline at high ligand in §3.5.

2.4 Reaction order

The reaction order (logarithmic sensitivity) $\nu_{S,x} = \partial \log S / \partial \log x$ (central difference, $\varepsilon = 10^{-3}$), computed for S_1, S_2 against L_1, L_2: two self-activation orders ($\nu_{S_1,L_1}, \nu_{S_2,L_2}$) and two cross-coupling orders ($\nu_{S_1,L_2}, \nu_{S_2,L_1}$).

2.5 Decision boundary and two-level heatmaps

The growth/defense switch is defined by $S_1 = S_2$ ($a_1 T_1 = a_2 T_2$). With everything else fixed, $S_2 - S_1$ increases monotonically with L_2, so there is a unique critical L_2^* (bisection in log space; the inner level uses the ODE steady state). This work gives **two-level** heatmaps, colored by dominance $\log_{10}(S_1/S_2)$ (defense-orange — white — growth-blue, `contourf` 17 levels + a black $S_1 = S_2$ boundary, inheriting the the earlier style):

- **Level 1 · ligand plane**: BL(L_1) × flg22(L_2), receptors fixed — "how the ligand environment toggles the switch".
- **Level 2 · receptor plane**: BRI1(R_1) × FLS2(R_2), ligands fixed — "how receptor expression toggles the switch", directly addressing the claim that "receptor stoichiometry is key".

2.6 Parameters

Realistic receptor stoichiometry (van Esse et al. [10]): $R_{1,\mathrm{tot}} = R_{2,\mathrm{tot}} = 2$ (≈ BRI1 62, FLS2 55 nM), $R_{A,\mathrm{tot}} = 1$ (≈ BAK1 30 nM) — receptors about twice the co-receptor. Ligand and affinity take working values that satisfy the "target functions": $K_{d1} = K_{d2} = 1$, $K_{1A} = K_{2A} = 2$ (anchor $\alpha_i(L = 1) = 2 \cdot 1/(1 + 1) = 1$), efficiencies $a_1 = 1,\ a_2 = 3$ (the defense downstream gain is stronger). **Priming terms removed**: no more K_h, σ this

work. Target-function check: no threat ($L_2 = 0$) $T_1 \approx 0.59 > 0.3$ ✓; with threat ($L_2 = 1$) $S_2/S_1 \approx 2.96 > 2$ ✓.

3 Results

3.1 ODE dynamics → steady state: a behavioral gallery

Fig. 1(a) shows the ODE time course: from the "all-free" initial condition, $T_1(t), T_2(t)$ monotonically approach steady state (dashed), with stronger threat (larger L_2) giving a higher defense-complex T_2 steady state and a more suppressed growth T_1. **These trajectories are genuine ODE integration**; their asymptotes agree with the the earlier algebraic fixed point to $\sim 10^{-7}$ (self-check: 300 random parameter sets, $\max \mathrm{rel}|T_{\mathrm{ODE}} - T_{\mathrm{alg}}| = 3.9 \times 10^{-7}$) — confirming "the model is dynamics" and that all the earlier steady-state conclusions are unchanged in the new framework.

The remaining panels are steady-state readouts: (b) signal curves S_1, S_2 vs L_2 — no threat gives high growth and near-zero defense, rising flg22 lets FLS2 take BAK1, and the two curves cross at the switch point $L_2^* \approx 0.158$ ($S_2/S_1 @ L_2 = 1 \approx 2.96$); (c) partitioning of shared BAK1 $T_1 + T_2 + F \equiv R_A$, the material basis of antagonism; (d) the dominance zero-crossing curve; (e) switch point vs defense efficiency a_2 — $a_2: 1 \to 10$ takes $L_2^*: 1 \to 0.039$; (f) switch point vs BAK1 total R_A — $R_A: 0.5 \to 2$ takes $L_2^*: 0.178 \to 0.121$ (more BAK1 → lower switch point → larger defense region; detailed in §3.6).

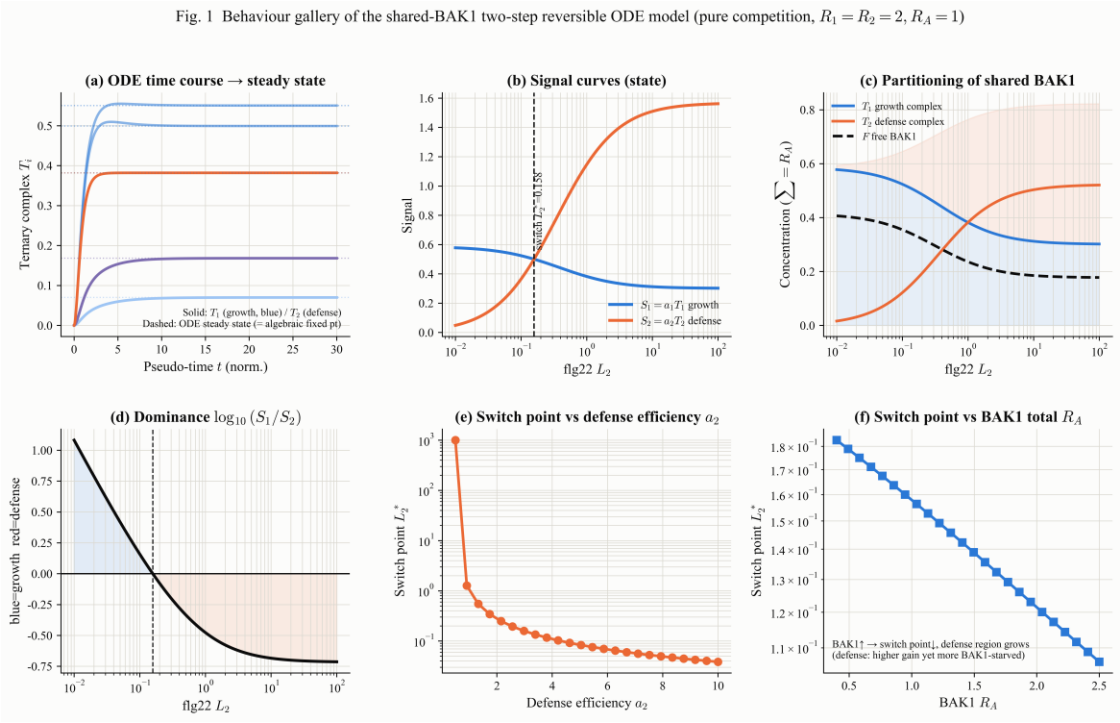

Fig. 1 Behaviour gallery of the shared-BAK1 two-step reversible ODE model (pure competition, $R_1 = R_2 = 2, R_A = 1$)

Fig. 1 Behaviour gallery of the shared-BAK1 two-step reversible ODE model (pure competition). (a) ODE time course approaching steady state (dashed = steady state =

algebraic fixed point); (b) signal curves (state); (c) BAK1 partitioning; (d) dominance; (e) switch point vs defense efficiency; (f) switch point vs BAK1 total.

3.2 Reversibility saturation: one-step linear vs two-step reversible

Restoring the ligand–receptor step to reversible changes the **high-ligand behavior** of the effective affinity (Fig. 2): (a) $\alpha(L)$ goes from "linear divergence" to "capping at $K_{iA} = 2$"; (b) the growth signal $S_1(L_1)$ tends to 2.0 in the one-step version and to ≈ 0.72 in the two-step; (c) the reaction order $\nu(S_1, L_1)$ falls off faster at the high end in the two-step version. Physically: strong binding ensures effectiveness already at low ligand (α stays large), while reversibility ensures the signal stops rising once the receptor is saturated. This "strong yet bounded" saturation underlies all subsequent heatmaps and reaction orders.

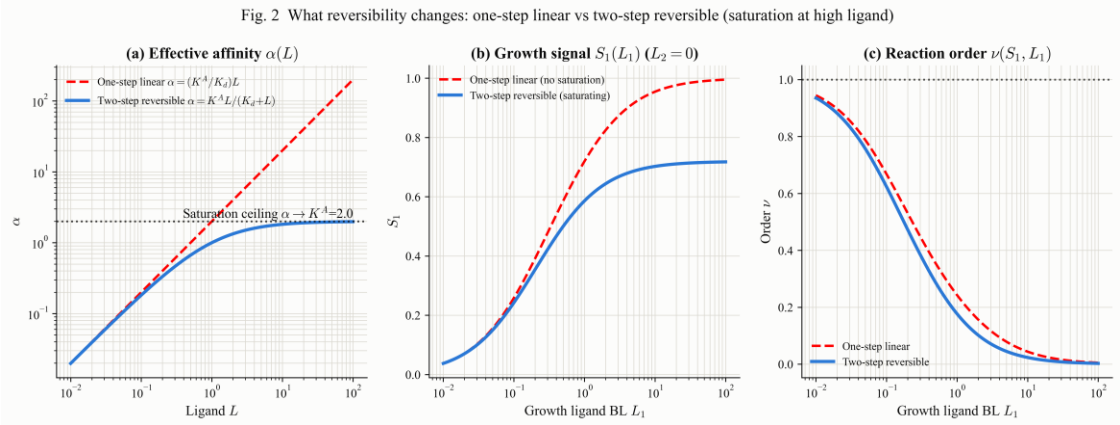

Fig. 2 What reversibility changes. (a) Effective affinity $\alpha(L)$: one-step linear divergence vs two-step reversible capping at K_{iA}; (b) growth signal $S_1(L_1)$ ($L_2 = 0$) one-step $\to 2.0$ vs two-step $\to 0.72$; (c) reaction order $\nu(S_1, L_1)$.

3.3 Two-level decision heatmaps

Fig. 3 gives the two-level decision heatmaps. **(a) Ligand plane**: BL(L_1) × flg22(L_2), the black line is the $S_1 = S_2$ boundary; at the working point ($L_1 = 1$) the switch is $L_2^* \approx 0.158$ — below-left is growth-dominated, above-right is defense-dominated. **(b) Receptor plane**: fixed ligand $L_1 = L_2 = 1$, scan BRI1(R_1) × FLS2(R_2). The switch boundary falls at $R_1^*(R_2 = 2) \approx 6.0$, i.e. $R_1^*/R_2 \approx 3 = a_2/a_1$ — **to switch to growth dominance, BRI1 must outweigh FLS2 by the efficiency factor** (the $a_2 = 3$ efficiency advantage of the defense pathway needs a 3× BRI1 amount to offset it). The working point $R_1 = R_2 = 2$ lies on the defense side: with equal receptors and equal ligand, the higher-efficiency defense pathway wins.

The two levels are complementary: the ligand plane answers "given receptor expression, what pathogen/hormone environment favors growth or immunity"; the receptor plane answers "given the environment, what receptor expression ratio toggles the switch" — the latter being the direct lever for resistance breeding.

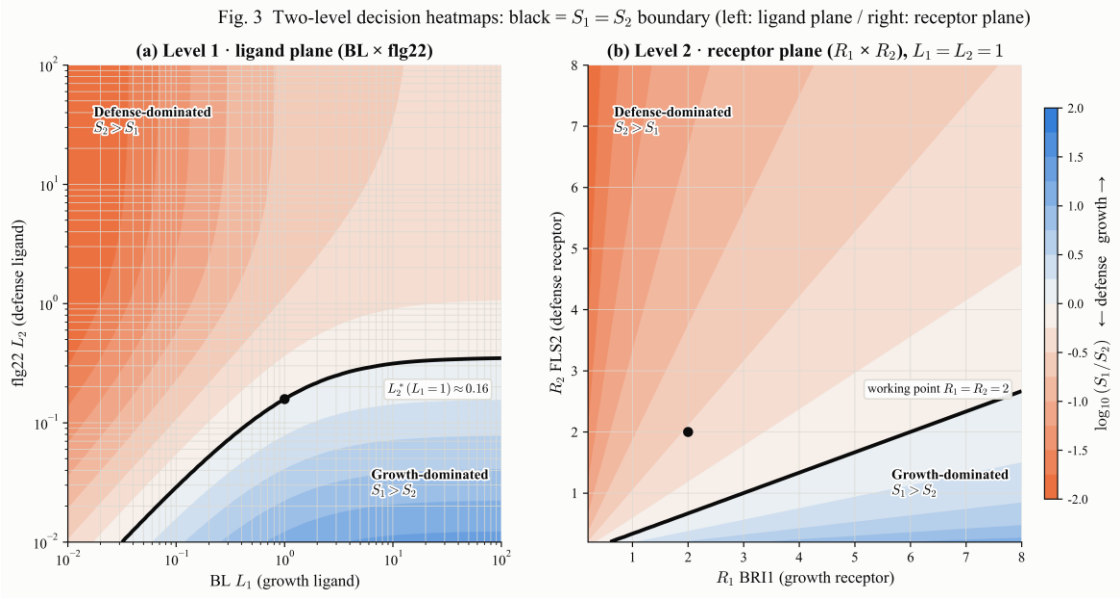

Fig. 3 Two-level decision heatmaps (black = $S_1 = S_2$ boundary). (a) Level 1 · ligand plane BL × flg22; (b) Level 2 · receptor plane BRI1 × FLS2 ($L_1 = L_2 = 1$), boundary $R_1^* \approx 3R_2$ matching the efficiency ratio a_2/a_1.

3.4 Three BRI1:FLS2 receptor ratios

Fix FLS2=2 and vary only BRI1: how does the receptor ratio move the **ligand-plane** switch boundary (Fig. 4)? High BRI1 (4:1, $R_1 = 8$) → boundary shifts right, more flg22 is needed to switch to immunity ($L_2^* = 2.2$); equal (1:1) → $L_2^* = 0.158$; low BRI1 (1:4, $R_1 = 0.5$) → boundary shifts left, very little flg22 switches to immunity ($L_2^* = 0.026$). That is, **more BRI1 pushes the switch boundary toward "a stronger threat is needed to turn defensive"**. Breeding implication: moderately down-regulating BRI1 (or up-regulating FLS2) shifts the boundary left, letting the plant enter immunity dominance under weaker pathogen signals, at the cost of slightly lower basal growth — a quantitative expression of the "growth–immunity trade-off".

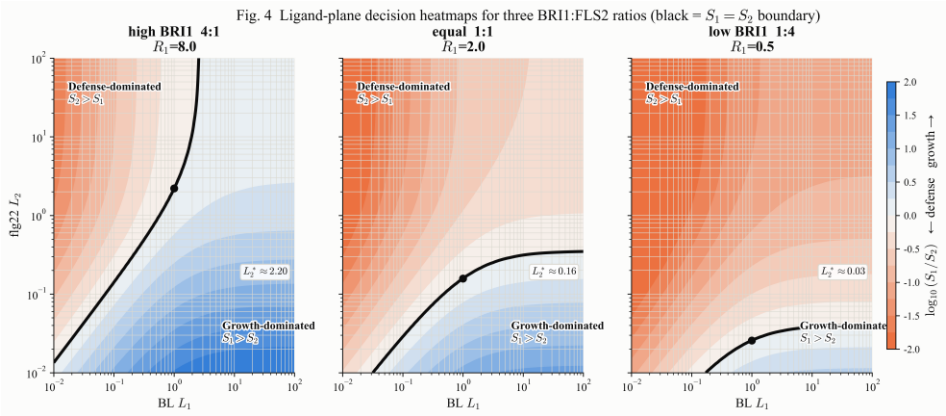

Fig. 4 Ligand-plane decision heatmaps for three BRI1:FLS2 ratios (black = switch boundary, ● = switch point at $L_1 = 1$).

3.5 Reaction order: the quantitative signature of antagonism

The geometric meaning of the reaction order is shown in Fig. 5: it is the slope of the log–log curve ($\nu = 1$ first-order unsaturated, $\nu \to 0$ saturated, $\nu < 0$ inhibitory). The four reaction orders of this system form a 2×2 — the two diagonal self-activation orders are positive, and the key off-diagonal ν_{S_1,L_2} turns negative under threat, the antagonism signature.

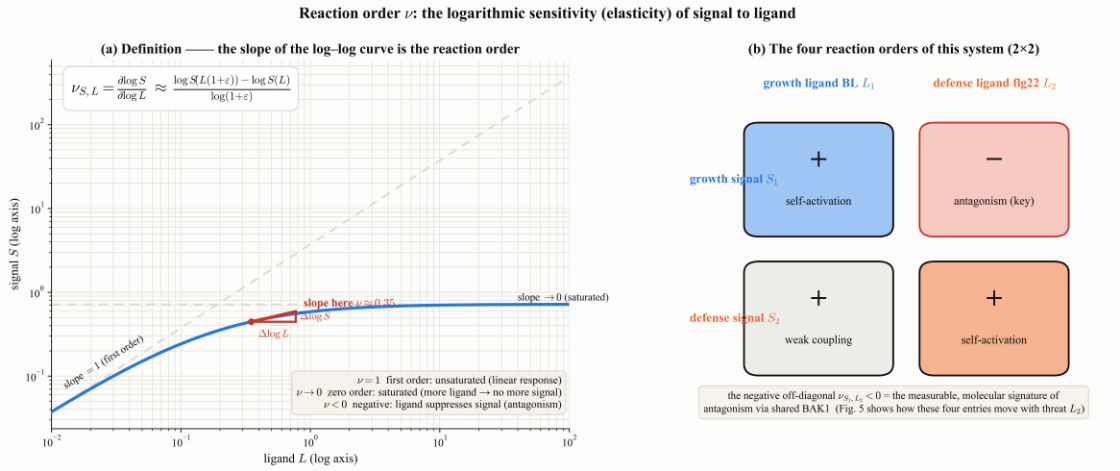

Fig. 5 Definition and meaning of the reaction order $\nu_{S,L} = \partial \log S / \partial \log L$. *(a) the slope of the log–log curve is the reaction order, with the formula and the three regimes* $\nu = 1/0/< 0$*; (b) the 2×2 of the system's four reaction orders: diagonal = self-activation (+), key off-diagonal* $\nu_{S_1,L_2} < 0$ *= the shared-BAK1 antagonism signature.*

Fix $L_1 = R_A = 1$, scan the threat L_2, and compute the four reaction orders (Fig. 6; characteristic-point readings in Table 1).

Table 1 Reaction orders vs threat level (two-step ODE model, $R_1 = R_2 = 2, R_A = 1, K_{di} = 1, K_{iA} = 2, a_1 = 1, a_2 = 3$)

Threat L_2	ν_{S_1,L_1} growth self-act.	ν_{S_1,L_2} cross (repressed by flg22)	ν_{S_2,L_2} defense self-act.
Low (10^{-3})	$+0.18$	≈ 0.00	$+0.96$
Mid (1)	$+0.26$	$\mathbf{-0.15}$	$+0.25$

Key points: (1) **the cross reaction order ν_{S_1,L_2} goes from 0 to negative under threat** (global minimum ≈ -0.16 @ $L_2 \approx 0.56$) — adding flg22 actively suppresses the growth signal. This is the molecular-level, measurable signature of "shared-BAK1" antagonism. (2) **Defense self-activation drops from** $+0.96$ **to** $+0.25$ — at low flg22 the defense is nearly first-order (unsaturated), and as flg22 rises the ligand–receptor step saturates ($\alpha_2 \to K_{2A}$, §3.2), sharply bending the order.

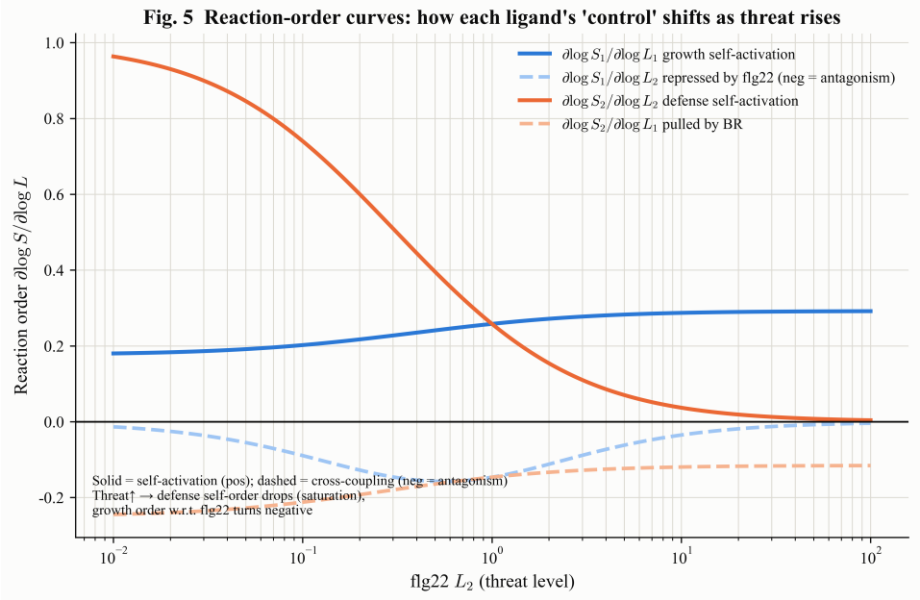

Fig. 6 Reaction-order curves. Solid = self-activation (positive); dashed = cross-coupling (negative = antagonism). As threat rises, the growth sensitivity to flg22 turns negative and the defense self-order bends down due to saturation.

3.6 Decision phase diagram: more BAK1, larger defense region

Three BAK1 totals $R_A = 0.5,1,2$ (Fig. 7): **more BAK1 → the black line moves down, the defense-dominated region expands** — at fixed $L_1 = 1$, L_2^* decreases monotonically with R_A ($0.178 \to 0.158 \to 0.121$). Reason: the defense pathway is more efficient ($a_2 = 3$) and most BAK1-starved at low L_2, so marginal BAK1 is converted to defense signal with a larger relative gain. This restates van Esse's "BAK1 is not BR-limiting in WT" as: adding BAK1 does not boost growth (the marginal resource flows to defense); wild-type growth dominance relies on low L_2, not on abundant BAK1.

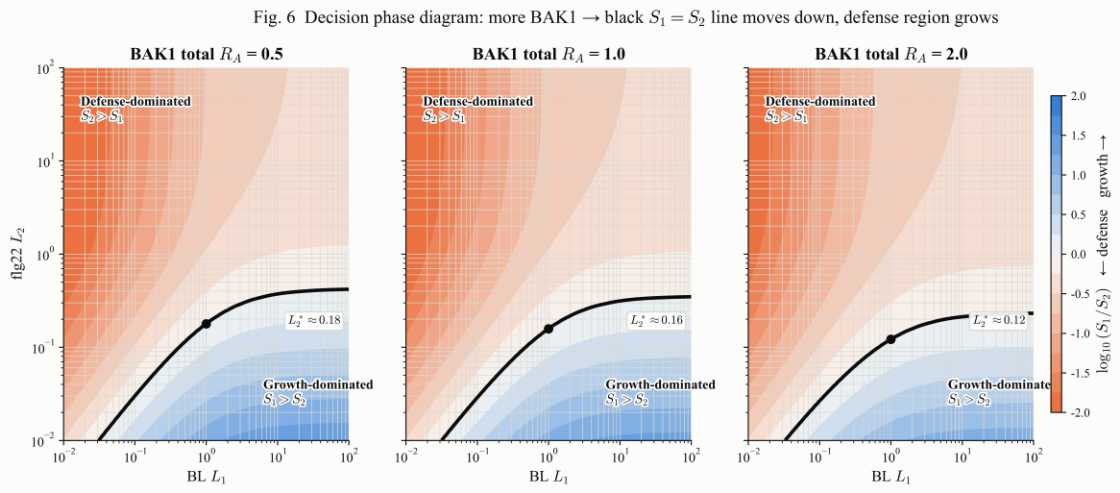

Fig. 7 Decision phase diagram (small multiples). Increasing BAK1 R_A → the black line moves down, the defense region expands.

3.7 Total-signal surface: total output under the BAK1 quota

How much total signal $S = S_1 + S_2$ does a cell emit at a given (L_1, L_2)? Because the two pathways compete for the same limited BAK1 pool ($T_1 + T_2 \leq R_A$), this sum is **bounded and non-monotone** (Fig. 8): (i) **the surface peaks at the pure-defense corner** ≈2.16 (= $a_2 \cdot T_{2,\max}$; the defense downstream efficiency is 3× growth), while the pure-growth corner is only ≈0.72 — the ratio of the two ends is proportional to a_2/a_1. (ii) **Mutual-inhibition signature**: under high threat, adding BL pulls BAK1 from high-efficiency defense ($a_2 = 3$) to low-efficiency growth ($a_1 = 1$), lowering the output per unit BAK1, so the total signal **drops instead of rising** ($L_2 = 10$ row: peak ≈2.10 → ≈1.68 at high BL). The plainest illustration: **stimulating both pathways fully (L_1, L_2 both maxed) gives a total signal ≈1.72, lower than stimulating defense alone (≈2.16)** — on a shared resource, growth and immunity are genuinely zero-sum; neither can "have it both ways". That is, S is not a monotone function of ligand but a surface shaped by the BAK1 quota and the two pathways' efficiencies.

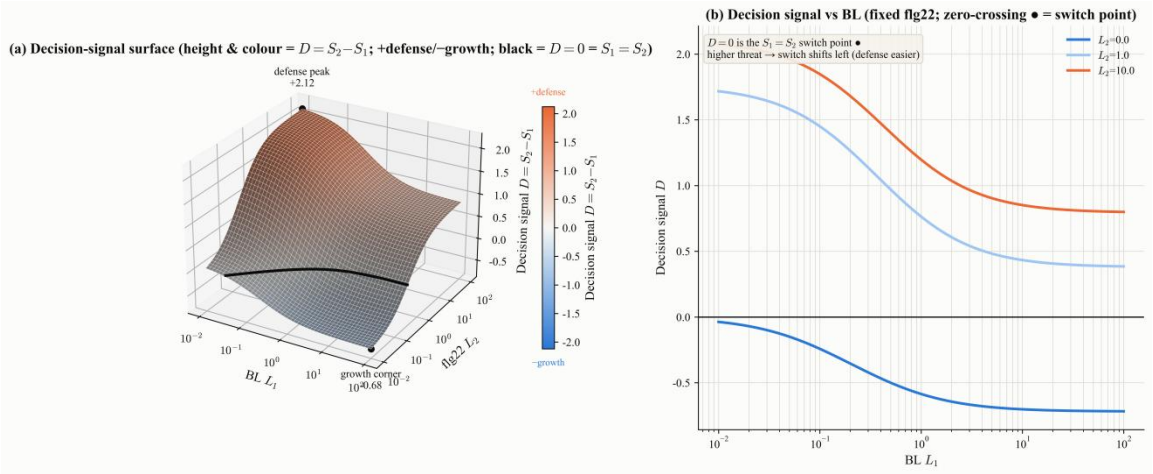

Fig. 8 Total-signal surface. (a) $S(L_1, L_2) = S_2 - S_1$ (height = total signal, color = dominance, floor black line = boundary); (b) at fixed flg22, adding BL makes the total signal drop at high BL (mutual inhibition).

3.8 Signal flow field

Treat the total signal $S(L_1, L_2)$ as a landscape and draw the streamlines of its gradient ∇S (Fig. 9): the low-ligand corners are high-sensitivity "sources" (fastest flow), and the saturated regions are stagnant "sinks". The non-trivial structure is on the defense-saturated, high-BL edge: here $\partial S / \partial L_1 < 0$, so the flow **reverses** in the L_1 direction (adding BL lowers the total signal — the §3.7 dip signed on the flow field) and the streamlines are pushed away. The overlaid yellow line $S_1 = S_2$ cuts the landscape into two regions.

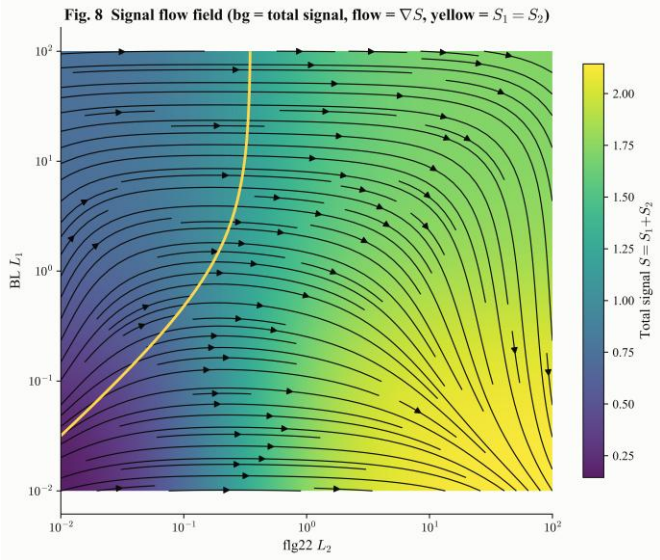

Fig. 9 Signal flow field. Background = total signal (viridis), black streamlines = ∇S, yellow line = $S_1 = S_2$ boundary.

3.9 Three antagonistic phenomena: pure competition suffices

Back to one of the project's starting points — can the model explain Belkhadir et al. [13] antagonistic phenomena? Under realistic stoichiometry, **the pure-competition ODE model reproduces three** (Fig. 10; @$L_2 = 10$ readout T_2/WT):

Table 2 Three antagonistic phenomena (two-step ODE pure-competition model, $R_1 = R_2 = 2, R_A = 1$)

Phenomenon	Perturbation	T_2/WT (pure competition)	Observed
BRI1-OE suppression	$R_1 \times 8\ (= 16)$	$\mathbf{0.34}$ (↓)	↓
+BAK1 rescue	$R_A \times 3\ (= 3)$	$\mathbf{2.42}$ (↑)	↑
High-BR suppression	$L_1 \to 100$	$\mathbf{0.82}$ (↓)	↓

The mechanism unifies as **stoichiometric sequestration**: BRI1 overexpression / high BR both make BRI1 sequester more BAK1, squeezing defense → T_2↓; adding BAK1 refills the squeezed pool → T_2↑. The key precondition is the realistic ratio $R_1 > R_A$ (receptors more abundant than the co-receptor), otherwise sequestration is too weak and high-BR suppression is missed (consistent with the the earlier diagnosis, and quantitatively confirmed in §3.10 where R_1/R_A is its top driver). **No priming term is introduced this work** — the two synergistic-side phenomena (*sud1* enhancement, BRZ inhibition) need activity-dependent mechanisms, beyond the pure-competition scope here.

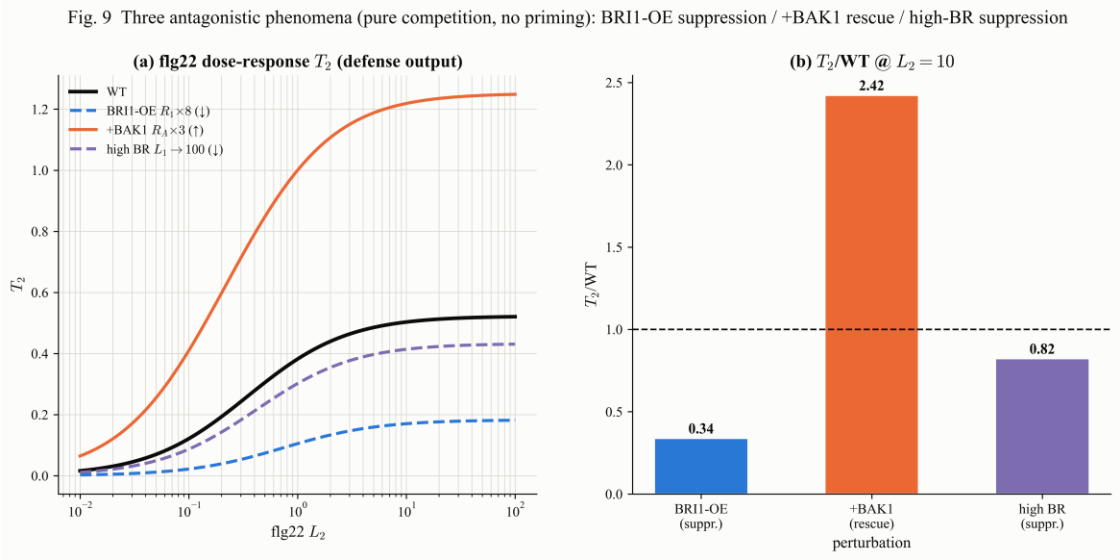

Fig. 10 Three antagonistic phenomena (pure competition). (a) flg22 dose–response T_2 for five genotypes/treatments; (b) T_2/WT at $L_2 = 10$.

3.10 Which factor drives which output: parameter-sampling sensitivity

Log-uniform sampling of 6 parameters (a_2, K_{2A}, K_{1A}, K_{d2}, K_{d1}, R_1/R_A; $N = 3000$, fixed $a_1 = 1, R_A = 1, R_2 = 2$; each set computes the switch point L_2^*, the three-phenomenon T_2/WT, and the total-signal ceiling, all by ODE integration), ranking the top drivers by Spearman correlation (Fig. 11). Full correlation matrix (rows = outputs, columns = parameters; **bold** = that output's top factor):

Output Param	a_2	K_{2A}	R_1/R_A	K_{d2}	K_{d1}	K_{1A}
Switch L_2^*	−0.50	−0.37	**+0.54**	+0.28	−0.19	+0.37
BRI1-OE T_2/WT	−0.02	+0.33	**−0.67**	−0.05	+0.27	−0.58
+BAK1 T_2/WT	+0.03	**−0.67**	+0.41	+0.07	−0.22	+0.52
High-BR T_2/WT	−0.02	+0.23	**−0.75**	−0.03	−0.37	−0.42
Signal ceiling	**+0.94**	+0.21	+0.07	0.00	+0.01	+0.05

Two conclusions:

(1) The three phenomena are 100% reproduced and share one mechanism — the strength of BRI1's sequestration of BAK1. Across 3000 random parameter sets, all three antagonistic phenomena appear in the correct direction (OE suppression, +BAK1 rescue, high-BR suppression all 100%), showing that the pure-competition mechanism is robust for these three and does not depend on specific parameter calibration. Mechanistically: BRI1 overexpression and high BR are both driven by R_1/R_A (-0.67, -0.75) and the BRI1–BAK1 affinity K_{1A} (-0.58, -0.42) (high BR also by the

BL–BRI1 binding K_{d1}, -0.37: stronger binding → deeper sequestration → stronger suppression); +BAK1 rescue is exactly the **reverse** — the stronger the sequestration (R_1/R_A ↑, K_{1A} ↑), the more rescue ($+0.41$, $+0.52$), and the weaker the FLS2–BAK1 affinity (K_{2A} ↓), the more starved the baseline and the larger the rescue room (-0.67). So "OE/high-BR suppression" and "+BAK1 rescue" are two sides of the same coin, both set by "BRI1's ability to grab BAK1".

(2) The knobs divide cleanly and are independently measurable. The switch point L_2^* is under "mixed control" — receptor stoichiometry R_1/R_A ($+0.54$), defense efficiency a_2 (-0.50), and both affinities K_{1A} ($+0.37$), K_{2A} (-0.37) together, none dominant; the total-signal ceiling is set almost solely by a_2 ($+0.94$) (the ceiling = the defense pathway's full-load output, proportional to its downstream efficiency). Thus three independently perturbable biological quantities each have their own job: **receptor expression ratio R_1/R_A gates whether antagonism occurs, downstream efficiency a_2 gates total capacity and switch difficulty, and co-receptor affinity K_{iA} gates the saturation position and switch point** — a testable structure of the model, also suggesting experiments along these three axes.

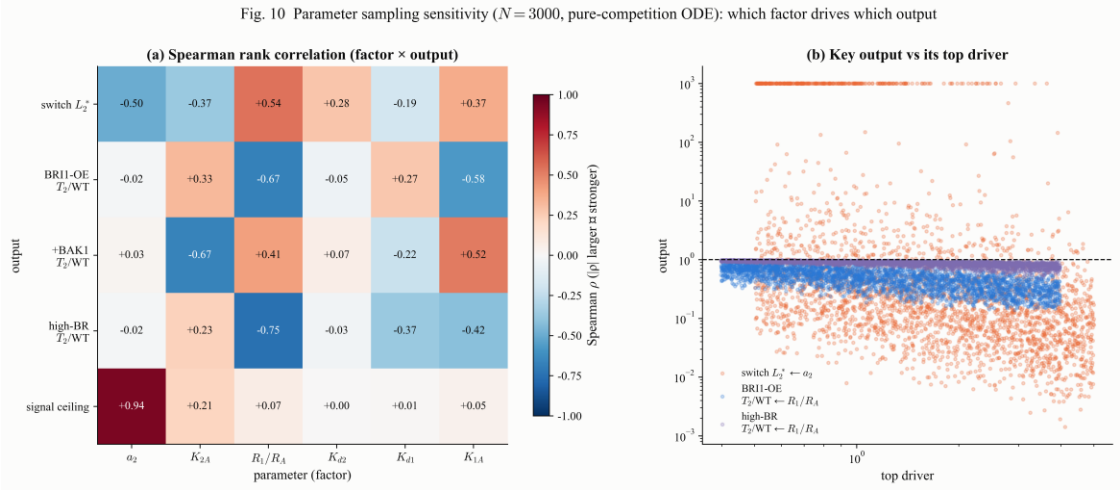

Fig. 11 Parameter-sampling sensitivity ($N = 3000$, pure-competition ODE). (a) Spearman correlation heatmap of factor × output; (b) key outputs vs their top drivers.

4 Discussion

The model is ODE dynamics, not an algebraic shortcut. This work writes the two-step reversible competition as an explicit mass-action ODE and integrates it to steady state; the time course (Fig. 1a) monotonically approaches the fixed point and matches the the earlier algebraic solution to $\sim 10^{-7}$. This turns "BAK1 competition" from a steady-state assertion into a visible process, and means that all results (heatmaps, phase diagrams, total-signal surface, flow field, sampling) come from one dynamics rather than separate algebraic special cases. Reversibility is explicit here as the denominator of $\alpha_i = K_{iA}L_i/(K_{di} + L_i)$ — the "strong yet bounded" saturation is the common root of the reaction-order decline and the total-signal cap.

Two heatmaps = two adjustable knob planes. The ligand plane answers "how the environment toggles the switch"; the receptor plane answers "how receptor expression toggles it". The latter gives a clean rule: at fixed ligand the switch boundary lies at $R_1^* \approx (a_2/a_1)R_2$ — for growth to regain dominance, BRI1 must outweigh FLS2 by the efficiency factor. This rule takes "receptor stoichiometry is key" from a sampling correlation (§3.10) to a readable figure, and points directly at breeding: adjusting the BRI1:FLS2 expression ratio translates the working point relative to the boundary on the receptor plane.

Unifying the two camps (continuing the earlier, now supported by the ODE and the three-level heatmaps). "BAK1 is not limiting" (van Esse/Albrecht) and "BAK1 is the coupling hub" (Belkhadir) are two views of the same decision surface: adding BAK1 lowers S_1/S_2 and expands the defense region (Fig. 7) — BAK1 is not limiting for **growth** (more does not boost growth) precisely because it is the **rate-limiting resource for defense**. The negative cross reaction order (§3.5) and the adjustable ligand/receptor two-level boundary (§3.3–3.4) are the quantitative carriers of this unification.

Three phenomena, one mechanism. §3.9 unifies the three antagonistic phenomena under **stoichiometric sequestration**, with no priming. This is consistent with Belkhadir's discrimination using *35S::BRI1* (amount↑). This work deliberately narrows to pure competition: the two synergistic-side phenomena (*sud1* enhancement, BRZ inhibition) point to activity-dependent mechanisms and are left for future extension within the ODE framework (e.g. adding a BRI1-kinase-activity modulation term to a_i or K_{iA} would naturally introduce priming at the kinetic level, without returning to steady-state algebra).

Predictions and limitations. (i) The negative cross order of §3.5 is experimentally testable: along a flg22 gradient, measure BRI1 and FLS2 reporters simultaneously; the former should show a negative logarithmic sensitivity to flg22. (ii) The receptor-plane $R_1^* \approx 3R_2$ of §3.3 is testable by BRI1/FLS2 expression gradients. (iii) Parameters are still normalized; calibration needs experimental data (measured BL–BRI1 $K_d \approx 7.4$ nM, etc.); (iv) the decision criterion $S_1 = S_2$ takes equal signal weights; if the downstream readout is nonlinear, the boundary bends further.

Appendix A: Steady-state fixed point of the ODE and Euler convergence

Steady-state simplification. From $\dot{T}_i = 0$, $T_i = K_{iA}C_iF$; from $\dot{C}_i = 0$ and substituting, $C_i = R_i^{\text{free}}L_i/K_{di}$. Together with $R_{i,\text{tot}} = R_i^{\text{free}}(1 + L_i/K_{di}) + T_i$, solve

$$T_i = \frac{K_{iA}(L_i/K_{di})\,R_{i,\text{tot}}\,F}{(1 + L_i/K_{di}) + K_{iA}(L_i/K_{di})F} = \frac{\alpha_i R_{i,\text{tot}}F}{1 + \alpha_i F}, \quad \alpha_i = \frac{K_{iA}L_i}{K_{di} + L_i}$$

the the earlier algebraic fixed point. Hand check ($L_1 = 1, L_2 = 0, K_{d1} = 1, K_{1A} = 2, R_{1,\text{tot}} = 2, R_A = 1$): $\alpha_1 = 1$, $T_1 = 2F/(1 + F)$, $F = 1 - T_1 \Rightarrow T_1 = 2 - \sqrt{2} \approx 0.586$, consistent with ODE integration.

Euler convergence. The system $\dot{\boldsymbol{x}} = \boldsymbol{f}(\boldsymbol{x})$ is dissipative in the positive orthant (column-sum diagonally dominant Jacobian, eigenvalues with negative real part), so a unique globally stable steady state exists. Explicit Euler $\boldsymbol{x}_{n+1} = \boldsymbol{x}_n + \Delta t\, \boldsymbol{f}(\boldsymbol{x}_n)$ converges monotonically for $\Delta t < 2/\rho$ (ρ = spectral radius), and the Euler fixed point ($\boldsymbol{f} = \boldsymbol{0}$) is the ODE fixed point. Per-cell adaptive $\Delta t_i = 1.2/\rho_i$ keeps stiff cells from slowing the whole; self-checks show $\max \mathrm{rel}|T_{\mathrm{Euler}} - T_{\mathrm{alg}}| \approx 4 \times 10^{-7}$ under random parameters.

Acknowledgments

This work is developed during the 2026 PEBBLE BioFusion Workshop at Westlake University in Hangzhou, China, from July 24th to August 4th. We thank the teaching assistants Wenqin Zhou, Ruoqing Zhang, and Yihang Ding for their patient guidance throughout the workshop, and we thank the workshop for giving us, students from a purely biological background, the opportunity to engage with mathematics and computer science.

References

[1] B. Huot, J. Yao, B. L. Montgomery & S. Y. He. Mol. Plant 7(9):1267–1287, 2014.

[2] Y. Belkhadir, L. Yang, J. Hetzel, J. L. Dangl & J. Chory. Trends Biochem. Sci. 39(10):447–456, 2014.

[3] M. Koornneef & D. Meinke. Plant J. 61(6):909–921, 2010.

[4] S.-H. Shiu & A. B. Bleecker. Proc. Natl. Acad. Sci. USA 98(19):10763–10768, 2001.

[5] U. Hohmann, K. Lau & M. Hothorn. Annu. Rev. Plant Biol. 68:109–137, 2017.

[6] K. H. Nam & J. Li. Cell 110(2):203–212, 2002.

[7] D. Chinchilla et al. Nature 448(7152):497–500, 2007.

[8] C. A. Bücherl et al. Plant Physiol. 162(4):1911–1920, 2013.

[9] E. Smakowska-Luzan et al. Nature 553(7688):342–346, 2018.

[10] W. van Esse et al. Plant Physiol. 163(3):1472–1481, 2013.

[11] R. Großeholz et al. eLife 11:e73031, 2022.

[12] C. J. Su et al. Cell Syst. 13(5):408–425, 2022.

[13] Y. Belkhadir et al. Proc. Natl. Acad. Sci. USA 109(1):297–302, 2012.

[14] C. Albrecht et al. Proc. Natl. Acad. Sci. USA 109(1):303–308, 2012.

[15] Y. Sun et al. Science 342(6158):624–628, 2013.